

Nanotoxicological Assessments to Warranty the use of Functionalized Y_2O_3 Nanoparticles for Biomedical Applications

D. Chávez-García^{1,*}, K. Juárez-Moreno^{2,3,*}, R. Reyes¹, J. Barrera¹, G. A. Hirata²

¹Centro de Enseñanza Técnica y Superior (CETYS), Camino a Microondas Trinidad S/N Km. 1, Moderna Oeste, Ensenada, Baja California, C.P. 22860, México

²Centro de Nanociencias y Nanotecnología CNyN-UNAM, Km 107 Carretera Tijuana-Ensenada, C.P. 22860 Ensenada B.C., México

³CONACYT-CNyN-UNAM, Ensenada, México

✉ These authors contributed equally

*Corresponding authors: E-mail: dalia.chavez@cetys.mx (D. C.); Tel.: +52 (646) 116 4952
kjuarez@ens.cnyn.unam.mx (K. J.); Tel.: + 52 (646) 175 0650 ext 720

DOI: 10.5185/amlett.2020.121583

This study is a summary of our results on synthesis, functionalization and biomedical application of luminescent lanthanide doped nanoparticles with Y_2O_3 as host lattice. The nanoparticles (NPs) studied were Y_2O_3 and $Y_2O_3: Eu^{3+}$ and they are water-monodispersed, synthesized by the sol-gel method and surface modified to be biocompatible with a silica shell. The NPs were conjugated with amine groups and folic acid to detect specific cancer cells. We carried out a complete nanotoxicological evaluation of NPs in HeLa and MCF-7 cancer cells and fibroblast (L929) cell line. Our results corroborate the bio- and hemocompatibility of NPs. No *in vitro* inflammatory response mediated by macrophages was elicited and no genotoxic effect was scored by comet assay. Internalization of folic acid-functionalized NPs was detected by flow cytometry comparing the internal cellular complexity and the cytoplasmic localization of NPs was confirmed by confocal microscopy. We provide with more evidences to warranty the biosafety of down conversion nanoparticles based on $Y_2O_3: Eu^{3+}$ and functionalized with folic acid for further biomedical and bio-imaging applications.

Introduction

In recent years, the use of nanobiotechnology and nanomedicine with molecular intra- and intercellular processes is increasing, because the research is concentrated into the possibilities of controlling and manipulating cell processes, for example, by targeted transport of active substances or cancer cells bioimaging [1-3]. Functionalized and multifunctional nanoparticles (NPs) for medical applications are created for several applications such as imaging and diagnostics, genetic screening, tests for viral or bacterial infection and the first signs of diseases before symptoms are manifested, the development of medicines and vaccines, drug delivery, treatments for diseases such as diabetes, cancer, heart disease and targeted therapies, among others (Fig. 1)[4-6].

Several types of NPs and nanodevices are under investigation for diagnostic or medicinal purposes: quantum dots, nanoshells, nanospheres, gold nanoparticles, paramagnetic nanoparticles, luminescent nanoparticles and carbon nanotubes. The great advantage

of them is that their size and surface properties can be modified to optimize their pharmacokinetics for imaging of specific cells. The increased imaging specificity would significantly improve accuracy in diagnosis and an improved prognosis, also their photoluminescence (PL) properties, make them useful for single/multi-modal and single multi-functional molecular imaging [7-11].

The new bioimaging methods optimized by NPs can determine more accurately, than conventional methods, the presence, position, and size of tumors [12]. However, these methods are relatively new and the mechanisms by which the NPs can lead to toxicity are still in development. The lack of availability of detailed toxicology data on NPs or nanocarrier systems makes it difficult to evaluate their potential toxicity and also their impact on the environment [13]. The toxicity of nanoparticles depends on various conditions, including not only physicochemical properties of nanoparticles (e.g., size, shape, chemical composition, photoluminescence, etc.), but also physiological status (e.g., genetics, disease conditions, etc.) [14,15].

Table 1 shows several types of nanomaterials with cytotoxic and cellular uptake. For example, Park *et. al.*, [16] synthesized multifunctional carbon-based nanodots (C-dots) using atmospheric plasma treatment as a surface functionalization method to enhance C-dots' optical properties and antibacterial activities with strong fluorescence and low cytotoxicity. Yu *et. al.*, [17] analyzed the potential toxicological effects of nanoparticles, due to their ability to generate excessive amounts of reactive oxygen species (ROS). This resulted in the damage of biomolecules and organelle structures, which further cause necrosis, apoptosis, or even mutagenesis. Thus, the bioaccumulation of NPs can induce inflammation and immune responses, which result in cell injury, death, organ dysfunction, and ultimately stimulate the occurrence of numerous diseases, such as Alzheimer's, Parkinson's, liver inflammation, and dysembryoplasia. These issues have become more pressing with the wide-spread use of NPs. Therefore, broad nanotoxicological studies of given NPs are crucial to warranty their biosafety and further biomedical applications.

Table 1. Toxicity and cellular uptake of several NPs with different cancer cells.

Cell line	Size of NPs (nm)	Shape of NPs	Nanoparticle surface group	Cites
COS-1 kidney mammalian cells, and red blood cells,	2	Spheres	Quaternary ammonium, carboxylic acid	[18]
K562 human leukemia	4, 12, 18	Spheres	CTAB, citrate, cysteine, glucose, biotin	[19]
MV3 and BML, metastatic melanoma	1.4	Spherical cluster	Triphenylphosphine monosulfonate	[20]
HeLa cervix adenocarcinoma	65x11	Rods	CTAB, PEG	[21]
Baby hamster kidney cells BHK2, Human liver carcinoma Hep2G, Human lung carcinoma cells A549	33	Spheres	CTAB and citrate	[22]
Osteoblasts	60-140	Spheres	Bare	[23]
HEK293 cells	41±5	Spheres	Bare	[24]
Cell lymphoma	198 ± 9.01 nm	Bi-concave	Folic acid-glycine-poly-L-lactic acid	[25]
Mouse fibroblast L929, rat glioma cell line C6 and the human glioma cell line U251	96.3 nm	Spheroidal	Water-soluble polyhydroxylated fullerene	[26]
BEAS2B, THLE2, A549 and hep3B cell lines	2.3-6.3 nm	Spherical	Plasma treatment of C-dots-PEG	[16]

CTAB: cetyl trimethyl ammonium bromide;
PEG: polyethylene glycol

The following figure shows the process of the functionalization of the NPs and their penetration into the studied cells.

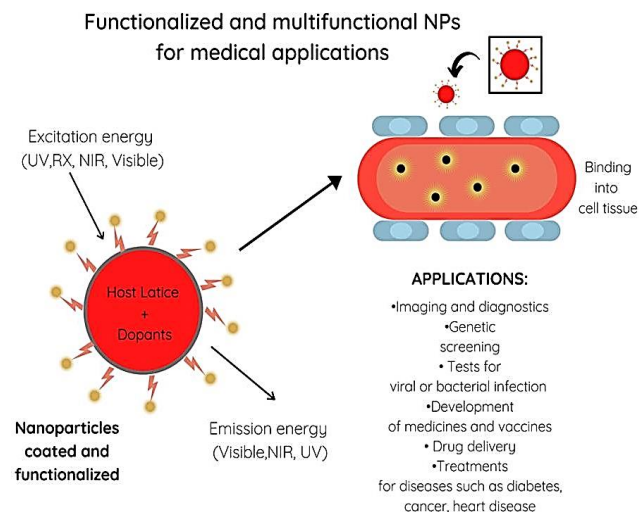


Fig. 1. Graphical representation of the functionalized NPs and their applications.

In order to bind and internalized into the cells, the NPs have to be coated for biocompatibility and also, they need functional groups that can bind to the surface receptor of the targeted cells, depending of the affinity or the applications, the functional groups on the surface may vary, some of the groups are in **Table 1**.

In this study, we synthesized, characterized and functionalized lanthanide downconversion nanoparticles (DCNPs) with the host lattice of Y_2O_3 . The biocompatibility was accomplished with a silica core-shell and the functionalization was done with amine groups NH_2 attached to folic acid ligands (FA). The Y_2O_3 -based biolabels can bind to receptors overexpressed in the membrane of cancer cells and then internalized by folate receptors (FR) on the cell membrane via endocytosis [27,28]. The FR is a high affinity membrane folate-binding protein and their localization is in the caveolae, the receptor internalization can be induced by receptor crosslinking. The over-expression of FR has been observed in various types of human cancers, such as: carcinomas, kidney, lung, mammary gland, brain and endometrium [27,29-33]. The DCNPs were internalized and observed into cervical (HeLa) and breast (MCF-7) adenocarcinoma cell lines by flow cytometry and confocal microscopy. To probe the bio- and hemocompatibility of DCNPs we used fibroblasts cells (L929), and erythrocytes from peripheral blood samples, and we tested the *in vitro* inflammatory responses on macrophages (RAW 264.7). We previously reported a nanotoxicological study of Y_2O_3 : Eu^{3+} (5% mol) DCNPs with MDA-MB-231, B16-F10 and RAW 264.7 cell lines [34], herein we present broader comparison of the Y_2O_3 -based DCNPs for biomedical applications.

Experimental

Materials

The chemicals used for the synthesis were: $Y(NO_3)_3$ (Alfa Aesar 99.9965%), $Eu(NO_3)_3$ (Alfa Aesar 99.9%) and tartaric acid ($C_4H_6O_6$ Aldrich, USA). For the silica-shell we used: TEOS (Tetraethyl orthosilicate, Sigma Aldrich, MO, USA), ammonium hydroxide (NH_4OH , Sigma Aldrich; MO, USA), IGEPAL surfactant (Sigma Aldrich, MO, USA). For the amino functionalization: APTMS, 3-Aminopropyl-trimethoxysilane (98%, Sigma Aldrich). For the FA functionalization: Folic acid (Sigma Aldrich; MO, USA), triethylamine (TEA, Sigma Aldrich, MO, USA), dimethyl sulfoxide (DMSO, Sigma Aldrich, MO, USA), N-Hydroxysuccinimide (NHS, 99% Sigma Aldrich, MO, USA) and N,N'-Dicyclohexylcarbodiimide (DCC, 99% Sigma Aldrich, MO, USA).

DCNPs synthesis and functionalization

The sol-gel (SG) synthesis was performed via tartaric acid [35] as previously reported. The precursor were mixed and stirred with deionized water and tartaric acid as a chelating agent for 24 h and then the mixture was heated $80^\circ C$ for 2h. Subsequently, the sol was heated at $120^\circ C$ until a gel was produced and dried to form the xerogel. The xerogel was annealed at $1200^\circ C$ for 2 h. The NPs obtained were $Y_2O_3: Eu^3$ (4% mol).

The functionalization was done with TEOS/APTMS, but first the DCNPs were sonicated because they tend to agglomerate with a high intensity ultrasonic processor (Sonics & Materials, Inc.) at 70% of the amplitude for 30 min with 20 mL of isopropanol/ethanol. The silica coating was performed by Stöber synthesis as reported [36,37], then the DCNPs were mixed with ammonium hydroxide, IGEPAL as surfactant and distilled water, they were constantly stirred for 24 h. The silica-coated DCNPs were centrifuged three times at 2000 rpm for 15 min at $24^\circ C$ and annealed at $900^\circ C$ for 2 h. Then they were mixed for 4 h in a solution of ethanol containing APTMS, TEOS and ammonium hydroxide.

The functionalization with FA ligands was also reported [38], it was done in a Schlenk system in a N_2 atmosphere. FA and TEA were added in 10 ml of dry DMSO and they were agitated for 2h at $37^\circ C$. Afterwards, a mixture was added to the solution with NHS and DCC and stirred at $37^\circ C$ in darkness for 12h to obtain FA-NHS. The mixture was filtered to separate the by-products. The DCNPs- NH_2 were dispersed in 25 mL of a carbonate/bicarbonate buffer (0.01M, pH 9.0) and ultrasonicated for 5 min. The FA-NHS solution was added to the DCNPs- NH_2 . The mixture was agitated in darkness for 2 h. Finally they were centrifuged at 6000 rpm for 15 min, washed three times with 45 mL of DMSO followed by five rinses with 45 ml of ethanol; they were vacuum dried overnight at $30^\circ C$.

Characterizations

The X-ray diffraction (XRD) was performed with a Philip's X'Pert diffractometer equipped with $Cu K\alpha$

($\lambda = 1.5406 \text{ \AA}$) radiation at a scanning rate of 0.5° . Measurements in a $2\theta = 10\text{--}80$ degree range was taken with a step size of $0.5^\circ/\text{min}$. The transmission electron microscopy (TEM) (JEOL JEM-2010) was used to characterize the morphology; it is operated at 200 kV. The photoluminescence (PL) spectra were analyzed by fluorescence spectrophotometer (Hitachi, FL-4500) equipped with 150 W Xe-lamp. The Fourier transform infrared spectroscopy (FTIR) was used to characterize the functional groups present on the surface of the DCNPs in the range of $400\text{--}4000 \text{ cm}^{-1}$ (Thermonicolet 1700). Zeta-potential measurements were conducted on Zetasizer Nano series (Nano-ZS, Malvern Instruments).

Cell culture and cell viability assay

Cell lines were obtained from the American Type Culture Collection (ATCC). Human cervix adenocarcinoma HeLa (CCL-2), human breast adenocarcinoma MCF-7 (HTB-22), murine fibroblasts L-929 (CCL-1) and mouse macrophages RAW 264.7 (TIB-71) cell lines, were cultivated in Dulbecco's Modified Eagle's Media (DMEM) supplemented with 10% v/v fetal bovine serum (FBS) (in the case of macrophages FBS was previously heat inactivated), 1.5 g/L of sodium bicarbonate, 1% v/v L-glutamine and 1% penicillin/streptomycin. Cells were grown until confluence at $37^\circ C$ and 5% CO_2 .

The reduction of 3-(4,5-dimethyl-2-thiazolul)-2,5-diphenyl-2H-tetrazolium bromide (MTT) was used to assess cell viability [39]. Briefly, cells were seeded at 10,000 cells per well in a 96-well plate for 24 h $37^\circ C$ and 5% CO_2 . Then, different concentration of DCNPs (1, 5, 10, 20, 40, 60 80, and 100 $\mu\text{g/mL}$) were added to each well in a final volume of 100 μL and incubated together with the cells for 24 h at $37^\circ C$ and 5% CO_2 . After this, cell were rinsed thrice with PBS 1x and MTT (0.5 $\mu\text{g}/\mu\text{L}$) was added to each well in 100 μL DMEM media and incubate for 4 h before absorbance reading in an ELISA plate reader (Thermo Scientific, USA). Background absorbance of cell test was measured at 690 nm and subtracted from the absorbance values at 570 nm. Positive control of cell viability was the cells cultured in DMEM media without DCNPs; while dimethyl sulfoxide was used to induce cell death (negative control). Absorbance values of positive control were used to calculate cell viability and normalize all obtained data from three independent experiments with internal triplicates.

Hemolysis assay

According to the ISO 10993-4:2017 one of the biological evaluations of medical devices with blood is the hemolysis quantification. To assess this, peripheral blood was obtained from a healthy donor and placed into a heparin-containing vacutainer tube (BD Biosciences), then the sample was centrifuged at 1750 rpm for 10 min at $25^\circ C$. The supernatant was discarded and the erythrocytes were obtained and rinsed once with 10 mL of NaCl (150 mM) and five times with PBS 1x (pH 7.4). Then, red blood cells were diluted 1:50 in PBS 1x and 270 μL of this sample was incubated for 1h at $37^\circ C$ with 30 μL of different

concentration of DCNPs. The erythrocytes diluted with PBS 1x were taken as a negative control, and the erythrocytes incubated with 20% (v/v) of Triton X-100 were taken as a positive control. After incubation with DCNPs, the samples were centrifuged at 3000 rpm for 5 min and the supernatant was collected. The optical density value (OD) of the supernatant was measured on a microplate reader (Multiskan Go, Thermo Scientific) at 541 nm. All experimental data were normalized to the mean value of positive control, which represents 100 % hemolysis; each sample was measured in triplicate and averaged. Then, each value was multiplied by 100 to obtain the percentage of hemolysis. The threshold of hemolysis or red blood cells is $\geq 5\%$ according to the standard.

Nitrite production

Nitric oxide produced by RAW 264.7 macrophages exposed to different concentrations of DCNPs was measured by the resulting nitrite ions using the Griess method [40]. Briefly, macrophages were seeded in a 96-well plate at a density of 10,000 cells per well for 24 h at 37°C and 5% CO₂. Then, different concentrations of DCNPs were added to each well in a final volume of 100 μ L and let them stand for 24 h at 37°C and 5% CO₂. After this, 20 μ L of cell media were taken and incubated in darkness with 80 μ L of sodium nitroprusside at 5 mM for 1 h at 37°C. One hundred microliters of Griess reagent (0.1% sulfanilamide and 0.1% N-(1-naphthylethylenediamine) were mixed with the sample and incubated for 15 min at 25°C. The absorbance of the samples was read at 540 nm and obtained values were compared with a standard curve of nitrite concentrations (from 1.67 to 100 μ M of sodium nitrite). Macrophages incubated with 200 ng of lipopolysaccharides extract (LPS) were taken as positive control of nitrite production.

Reactive oxygen species quantification by flow cytometry

Cells were incubated with different concentrations of DCNPs (1, 5, 10, 20, 40, 60, 80, and 100 μ g/mL) for 24 h. After this, they were washed with PBS 1x and incubated with 2',7'-dichlorofluorescein diacetate (30 μ M) for 90 min at 37°C and 5% CO₂. Then, the cells were centrifuged and resuspended in PBS 1X and subjected to flow cytometry analysis using a 488 nm excitation laser and 525 nm emission laser. Cells without DCNPs were used as a negative control, while cells grown with *tert*-butyl hydroperoxide (TBHP) (50 μ M) were considered as a positive control for generating higher superoxide levels. The fluorescence was recorded in a triplicate manner in three independent experiments for each sample, and was analyzed using the Attune NxT acquisition software version 3.2.1 (Thermo Fisher).

Genotoxicity assessment y comet assay

To assess the plausible genotoxic effect of DCNPs, we carried out the alkaline single cell gel electrophoresis assay also known as comet assay. HeLa, MCF-7 and L929 cell lines were incubated with 1,5,10,20, and 100 μ g/mL of

either bare DCNPs or FA-DCNPs for 24 h at 37°C and 5% CO₂. As a negative control, we used the same cell lines incubated in DMEM media without DCNPs. Afterward, cells were rinsed with PBS 1x and alkaline single cell gel electrophoresis was performed as previously reported [41]. One hundred comets were count for their classification of the length of the comet tail in regards to the DNA damage index. The analysis was carried out with the ImageJ free software (National Institutes of Sciences, USA).

Cellular uptake of DCNPs by flow cytometry and confocal microscopy

Internalization of DCNPs-FA in HeLa and MCF-7 cancer cells was carried out by flow cytometry and confocal microscopy, fibroblast cell line L929 was used as negative control due to the lack of FR on their cell membrane. For flow cytometry measurements, cell lines were seeded at a density of 50,000 cells in a 12-well plate for 24 h at 37°C and 5% CO₂. Then, 100 μ g/mL of FA-DCNPs were added to each well and incubated for 24 h at 37°C and 5% CO₂. After this, cells were rinsed thrice and detached from the plate by trypsinization and resuspended in 1 mL of PBS 1x to analyze them with an Attune NxT flow cytometry (Life Technologies). Data acquired consists of 50,000 events detected with forward scatter (FSC) and side scatter (SSC) beams. Uptake of DCNPs-FA into cells was carried out using the Attune NxT software by comparing the cell's granularity (SSC-H) with the same cell line without NPs treatment. Additionally, cellular uptake of DCNPs-FA into cancer cells was assessed by confocal microscopy using an inverted laser-scanning Olympus FluoView FV1000 (Olympus, London, UK). Cells were seeded on a poly-L-lysine (5 mg/mL) sensitized coverslip (0.13-0.17 mm) at a density of 50,000 cells, and incubated with 100 μ g/mL of DCNPs-FA. Nuclear staining was carried out as previously described by us [34]. Briefly, DCNPs was detected by red fluorescent protein (RFP) filter at λ_{exc} 478 nm and λ_{em} 660 nm. A plan achromatic 60x/1.48 N.A. oil immersion objective was used to visualize the cells and the images were analyzed with the FV10-ASW viewer version 4.2 from Olympus. Scale bar represents 50 μ m.

Statistical analysis

All the experiments were done in a threefold-independent manner with internal triplicates. The results were expressed as mean \pm standard deviation of three independent experiments. Data were evaluated by analysis of variance (ANOVA), followed by Tukey's multiple comparison test, using Graph Pad Prism 6.0 software. The results were considered statistically significant when $p < 0.05$.

Results and discussion

Physicochemical characterization

The XRD diffraction pattern of Y₂O₃ and Y₂O₃:Eu³⁺ (4% mol) synthesized by sol-gel are shown in **Fig. 2(a,b,c)**, they presented sharp and distinct peaks that demonstrates

crystalline NPs. The diffraction patterns in both samples correspond to the reference XRD database of pure cubic Y_2O_3 phase (JCPDS: 83-0927), **Fig. 2(c)**. The most intense peaks corresponding to hkl (222) were used to calculate the crystallite size of the NPs of $Y_2O_3:Eu^{3+}$ with the Scherrer's equation $D_p = (0.94 \lambda) / (\beta \cos\theta)$ where D_p is the average crystallite size, $\lambda = 1.5406 \text{ \AA}$, β is the line broadening in radians, and θ refers to the angle of the peak position. The crystallite size was 34 nm and the powder synthesized was nanocrystalline. Khachatourian *et. al.*, [42] reported a crystallite size of 19 nm for several concentrations of $Y_2O_3:Eu^{3+}$ from 1% from 1% to 13% molar, also Anh *et. al.*, [43] also reported a 10 nm crystallite size of $Y_2O_3:Eu^{3+}$ 5% molar. Gowd *et. al.*, [44] studied the effects of annealing temperature in the crystallite size, reporting 11.15 nm at 700° C and at 1400° C the size was 46.26 nm.

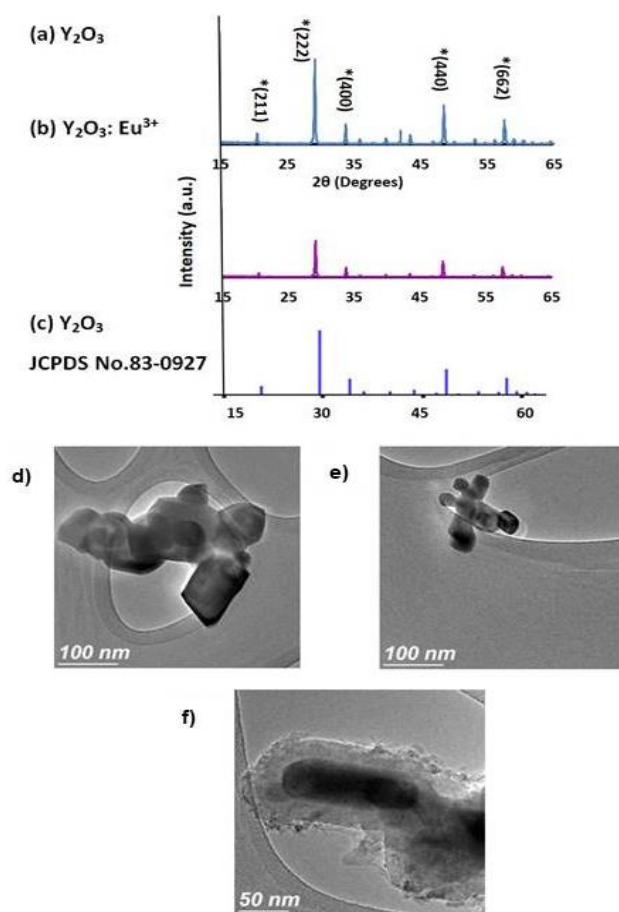


Fig. 2. X-ray diffraction patterns of (a) Y_2O_3 and (b) $Y_2O_3:4\%Eu^{3+}$ (4% mol) NPs compared with the (c) Y_2O_3 JCPDS No. 83-0927 database. TEM images of (d) bare Y_2O_3 (e) bare $Y_2O_3:Eu^{3+}$ (4% mol), (f) folic acid functionalized $Y_2O_3:Eu^{3+}$

The **Fig. 2(d)**, **Fig. 2(e)** and **Fig. 2(f)** are also showing TEM images of bare SG synthesized Y_2O_3 (**Fig. 2(d)**), $Y_2O_3:Eu^{3+}$ (**Fig. 2(e)**) and the FA functionalized DCNPs (**Fig. 2(f)**). The images showed spheroidal particles of approximately 80 nm size and at this stage they are agglomerated, thus, in order to functionalize them we used IGEPAL surfactant. **Fig. 2(f)** shows the silica shell of

DCNPs-FA approximately of 10 nm thick. Huang *et. al.*, [45] and Khachatourian *et. al.*, [42] reported and increasing of the size of the NPs with the Eu^{3+} concentration of about 13%, in our study the NP size was similar in Y_2O_3 with and without doping.

FTIR analysis of bare and doped NPs was previously reported [34]. The PL of excitation and emission spectra of NPs and $Y_2O_3:Eu^{3+}$ (4% mol) bare and functionalized DCNPs-FA are depicted in **Fig. 3**.

The photoluminescence (PL) emission spectra of 4% Eu^{3+} doped Y_2O_3 (excitation at $\lambda = 254 \text{ nm}$) showed the 613 nm characteristic red emissions. The PL spectra (**Fig. 3**) showed the emission broadband attributed to the transition $^5D_0 \rightarrow ^7F_2$, that corresponds to the charge transfer from $O^{2-} \rightarrow Eu^{3+}$ (**Fig. 3(a)** excitation spectra) due to the electronic transition between $O^{2-} 2p$ orbital to the unfilled $4f^6$ orbital of Eu^{3+} . The 5D_0 level will not be split into the crystal-field ($J=0$), so the emission transitions yields on the $7F_j$ levels [46-48].

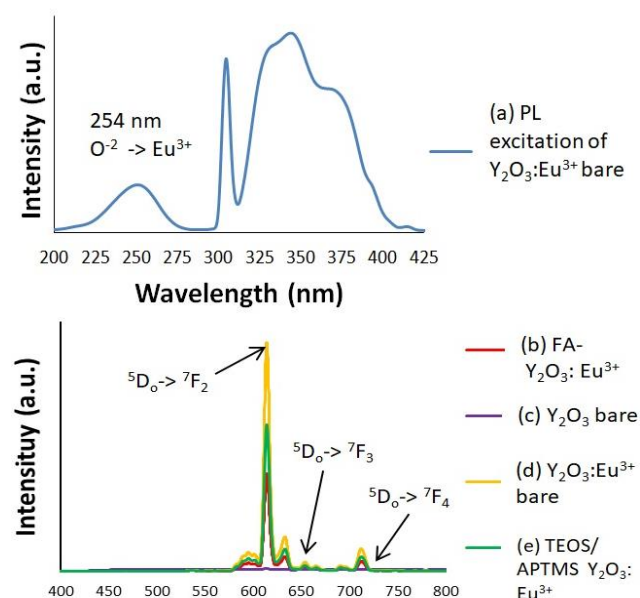


Fig. 3. (a) PL excitation spectra of bare $Y_2O_3:Eu^{3+}$ (4% mol) (blue); PL emission spectra at $\lambda=254 \text{ nm}$ ex. of (b) FA- $Y_2O_3:Eu^{3+}$ NPs (red), (c) bare Y_2O_3 NPs (violet), (d) bare $Y_2O_3:Eu^{3+}$ (4% mol) (orange) and (e) functionalized TEOS/APTMS $Y_2O_3:Eu^{3+}$ (4% mol) (green).

Nanotoxicological assessments

Nanotoxicological assessments of nanomaterials have become a trend especially in those with wide biomedical applications. Herein, we present the synthesis of down conversion NPs functionalized with folic acid to allow their active delivery to cervical and breast cancer cells, recognized to overexpress folic acid on their cell membranes [49]. The key parameters that drive *in vitro* toxicity studies of given nanomaterials are related to biocompatibility, genotoxicity and inflammatory responses. To achieve this, we carried out several *in vitro* nanotoxicological assessments. As shown in **Fig. 4**, we tested the cytotoxic effect of several concentrations of bare and DCNPs-FA in cervix (**Fig. 4(a)**) and breast (**Fig. 4(b)**) cancer cell lines and fibroblast L929 (**Fig. 4(c)**)

was used as a control of no malignant cell line. As observed, the bare DCNPs caused a slight toxicity of less than 25% in both cancer cell lines only after the following concentrations: 80 $\mu\text{g/mL}$ for HeLa and 60 $\mu\text{g/mL}$ for MCF-7 cells. However, no cytotoxic effect was detected in fibroblasts. After the functionalization of DCNPs with folic acid, their cytotoxic effect on all the three cell lines was negligible. These results confirm that functionalization of DCNPs with folic acid reduces their toxicity, making them biocompatible. This step is crucial for those nanomaterials that will be used as cell biolabels [50]. To further assess the biosafety of DCNPs a hemolysis test was performed. The release of hemoglobin by red blood cells is an indicator to evaluate the potential cell membrane damage caused by their interaction with DCNPs [51]. As depicted in Fig. 4(d) the percentage of hemolysis was measured by exposing erythrocytes to the same concentrations of bare DCNPs and DCNPs-FA previously used to assess cell viability. The results clearly demonstrated that the release of hemoglobin was below the threshold of 5% (red dotted line), because none tested concentration of both DCNPs exerted damage on the red blood cell membrane. Although there are many other hemocompatibility tests, the hemolysis assay plays a crucial role due to the abundance of this cell type in blood stream ($4\text{-}6 \times 10^6$ cells/ μL) and their importance in oxygen transportation, gas exchange, and sensing of osmotic pressure, among others [51]. Thus, bare DCNPs and DCNPs-FA can be considered to be hemocompatible according to the ISO 10993-4:2017. Further *in vitro* biocompatibility assays deals with inflammatory responses, most of them are led by macrophages and involve the production of nitric oxide (NO). A method to measure the production of NO is by the quantification of its by-products such as nitrites [52]. Some nanomaterials are capable to induce the increase of NO and nitrites, together they trigger cell death and inflammation [53,54]. Thus, we determine the concentration of nitrites produced by mouse macrophages that were incubated with different concentrations of bare and DCNPs-FA (Fig. 4(e)). Lipopolysaccharides (LPS) were used as an inductor of nitrites production and thus a positive control. In all the measured samples the concentration of nitrites was lower (≤ 20 μM) than in the positive control (~ 40 μM). Worth to mention is that the functionalization of NPs with folic acid reduced the production of nitrites significantly, especially in higher concentrations of DCNPs-FA such as 80 and 100 $\mu\text{g/mL}$. Nitric oxide is recognized as an important part of the immune system. Its increase has been correlated with high levels of nitrites in plasma upon inflammation [55]. Since the concentrations of nitrites measured by the macrophages exposed to DCNPs and DCNPs-FA were lower than the positive control, it is possible to confirm that none of the tested NPs induced any *in vitro* inflammatory responses exerted by nitrites. It is well known that NO and reactive oxygen species (ROS) are immunomodulators that regulate proinflammatory responses [52].

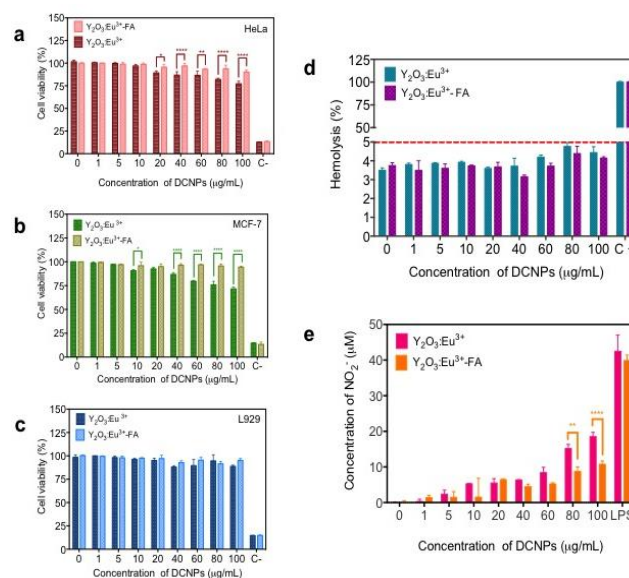


Fig. 4. Bio- and hemocompatibility of bare $\text{Y}_2\text{O}_3:\text{Eu}^{3+}$ and $\text{Y}_2\text{O}_3:\text{Eu}^{3+}$ -FA. Cell viability of (a) cervix adenocarcinoma HeLa, (b) breast cancer MCF-7 and (c) mouse fibroblast L929 cell lines exposed to different concentrations of bare and folic acid functionalized DCNPs. (d) Percentage of hemolysis elicited by the incubation of different concentrations of bare and DCNPs-FA on red blood cells. Dotted redline represents the threshold of allowed hemolysis (e) Quantification of nitrite production by mouse macrophages incubated with different concentrations of bare and functionalized DCNPs. Results are expressed as the mean \pm SD. Statistical significance of experiment was calculated using tow-way ANOVA (* $p < 0.05$; ** $p < 0.01$; *** $p < 0.001$ and **** $p < 0.0001$) with a Tukey's multiple comparison tests.

Thus, besides the quantification of NO, here we analyzed the induction of ROS generation by flow cytometry. As observed in Fig. 5 the level of ROS production in HeLa is similar between bare DCNPs and DCNPs-FA. However, cancer cell line MCF-7 incubated with higher concentrations of bare DCNPs (from 60 to 100 $\mu\text{g/mL}$) induced an increase of ROS generation (Fig. 5(a)). However, ROS production was not exerted by the incubation of breast cancer cells with DCNPs-FA, corroborating with this, that folic acid favors the biocompatibility of DCNPs. Finally, the generation of ROS production in L929 cell line was similar among all DCNPs concentration tested except for the higher concentration (100 $\mu\text{g/mL}$), but as expected, this was reduced after biological functionalization (Fig. 5(b)). ROS exert different signals inside the cells, most of them are involved in homeostasis, cell growth and differentiation. However, the intracellular increase of ROS led to oxidative stress as a defense mechanism towards a variety of inductors that also includes nanomaterials. It has been reported that metal and metal oxide nanoparticles among others, induce the outburst of ROS as the main mechanism of cytotoxicity [56]. ROS also are responsible for the induction of DNA damage, a phenomenon also attributed to some nanomaterials, especially metallic and metal oxide nanoparticles. Thus, having evaluated that DCNPs-FA are not capable of exacerbating the production of ROS in both cancer cells and fibroblasts, but that bare DCNPs

induce a slightly rise in ROS level at higher concentration; we evaluated the genotoxic effect of bare and DCNPs-FA in the cells lines. Different approaches can be used to determine genotoxicity, cell comet or alkaline single-cell electrophoresis has been recognized by the OECD as a standard method to evaluate single and double DNA strand fragmentations [57]. We measured the DNA damage index of cancer cells and fibroblasts incubated with different concentrations of bare DCNPs (Fig. 5(c)) and DCNPs-FA (Fig. 5(d)). The comparison of the scores of the comet tails from HeLa, MCF-7 or L929 cells without any treatment (basal DNA damage) were not statistically significant ($p > 0.05$) from those observed at lower (1, 5, and 10 $\mu\text{g/mL}$) or higher (20-100 $\mu\text{g/mL}$) concentrations of bare DCNPs and DCNPs-FA. Thus, there was not any significant DNA damage scored, and therefore we concluded that no genotoxic effect was exerted by the incubation of DCNPs with cell lines tested herein.

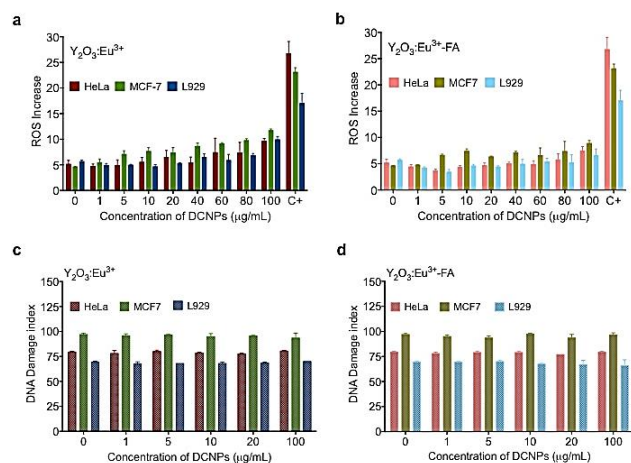


Fig. 5. Reactive oxygen species quantification and genotoxicity assessment of bare DCNPs and FA-DCNPs. ROS detected by flow cytometry in cervical cancer (HeLa), breast cancer (MCF-7) and mouse fibroblast (L929) cell lines, exposed to different concentrations of (a) bare DCNPs and (b) DCNPs-FA. Genotoxic effect of (c) bare-DCNPs and (d) DCNPs-FA was assessed by comet assay. Herein the DNA damage index is plotted for cancer cells and nonmalignant cells. Results are expressed as the mean \pm SD. Statistical significance of experiment was calculated using two-way ANOVA (* $p < 0.05$; ** $p < 0.01$; *** $p < 0.001$ and **** $p < 0.0001$) with a Tukey's multiple comparison tests.

Altogether, these results indicate that DCNPs-FA are bio- and hemocompatible; this is highly relevant when completing the nanotoxicological assessments of a given biolabel such as DCNPs. In this regard, we decide to evaluate whether the DCNPs-FA were capable of been internalized by cancer cells due to the overexpression of folic receptors on their cell membrane. Thus, firstly we determine the uptake of DCNPs-FA in cervical HeLa and breast MCF-7 cancer cells and compare it with L929 fibroblasts cells that lack FR on the cell membrane. To achieve this, we used flow cytometry to compare the cellular complexity (so-called granularity) of cells [58]. Incubated with the higher concentrations of DCNPs-FA (100 $\mu\text{g/mL}$) and compared it with the granularity of cells without NPs treatment. Cell complexity is measured by

flow cytometry using the side scatter beam (SSC-H), thus, the cell percentage that has internalized DCNPs-FA is detected with a different internal cell complexity due to the presence of vesicles containing nanoparticles [59]. As depicted in Fig. 6, when comparing the granularity of cervix (a) and breast (b) adenocarcinoma cell lines with and without DCNPs-FA, an increase of cell percentage complexity is observed. However, this is not found in fibroblast cells (c), due to the lack of folic acid receptors on their cell membrane, therefore these cells are not able to internalize DCNPs-FA and there is no change in internal cellular complexity as expected.

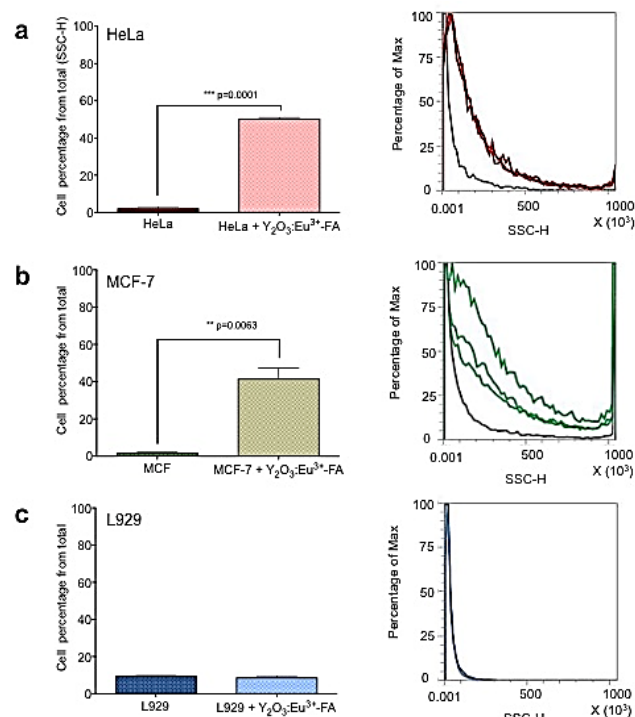


Fig. 6. Measurement of internalization of $\text{Y}_2\text{O}_3:\text{Eu}^{3+}$ -FA (DCNPs-FA) by flow cytometry. It is presented the comparison of cellular complexity (SSC-H) between (a) cervix HeLa, (b) breast MCF-7 and (c) fibroblasts L929 cell lines incubated with 100 $\mu\text{g/mL}$ of DCNPs-FA.

In attempts to provide more information regarding the internalization of these NPs and to corroborate these results we carried out confocal microscopy imaging to determine the intracellular localization of DCNPs-FA in HeLa and MCF-7 cells. It has been reported that cancer cells overexpress folic acid receptors in the cell membrane, thus active transport using folic acid as ligand has been successfully used before [60]. The confocal micrographs (Fig. 7) confirm that both cell lines were able to uptake DCNPs-FA. Although it is more evident the higher cytoplasmic localization of DCNPs-FA (red dots) in cervix adenocarcinoma cells than in breast cancer cells, this can be explained by the fact that HeLa expresses higher amounts of folic acid receptors on cell membranes than MCF-7 cells [49]. However, both cell lines were fully able to internalize DCNPs-FA as determined by flow cytometry and confocal microscopy. Therefore, it is possible to use these DCNPs as biolabels for cancer cells

that overexpress folic acid on their membranes. Herein we presented a complete physicochemical characterization study along with nanotoxicological evaluations to warranty the biosafety of DCNPs-FA to be used for further *in vivo* studies and biomedical applications.

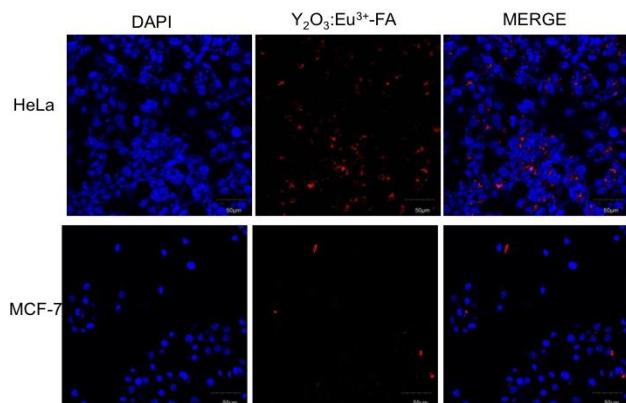


Fig. 7. Cellular localization of fluorescence $Y_2O_3:Eu^{3+}$ -FA nanoparticles in cancer cells. Confocal microscopy of cervical (HeLa) and breast (MCF-7) adenocarcinoma cell lines incubated with DCNPs-FA (red). DAPI depicts nuclear staining in blue. Scale bar represents 50 μm .

Conclusion

The $Y_2O_3:Eu^{3+}$ can produce efficient red emission (with the electronic transition $^5D_0 \rightarrow ^7F_2$) when excited with short wavelength UV at 254 nm. The XRD diffraction patterns showed a cubic structure with a crystallite size of 34 nm and a nanoparticles size around 80 nm \pm 10 nm. The DCNPs tend to agglomerate so the use of surfactant was needed to functionalize them. The functionalization was performed with TEOS/APTMS technique with a silica shell on the surface of the NPs and amino group bound with FA ligands. FA ligands bind to the folate receptor which is a selective tumor marker overexpressed in the cancer cells studied. Results from nanotoxicological analysis showed that DCNPs-FA are bio- and hemocompatible, because they do not interfere with cell viability and do not damage the red blood cell membrane. Moreover, they do not trigger any oxidative stress or *in vitro* inflammatory responses produced by macrophages, and importantly, they do not induce any genotoxic effect. These facts make them excellent candidates to be used as nanotools in the detection of circulating cancer cells or in other biomedical applications with especial focus in bioimaging. The importance of nanotoxicological studies is to provide evidence for a deeper understanding of the relationship between the physicochemical properties of NPs and the molecular/cellular responses exerted by them. These will contribute to tuning the design of suitable nanomaterials that can be safely used in biomedicine applications. A promising application is the use of DCNPs-FA as contrast agents for imaging studies. However, to accomplish this, *in vivo* toxicological studies in healthy and murine cancer models are needed. In the case of DCNPs-FA, our results support the usage of these nanotools for diagnosis applications, focusing on detecting of circulating cancer cells by flow cytometry.

Acknowledgements

K.J-M acknowledges the funding through CONACYT project 269071 and Cátedras CONACYT No. 53. The authors acknowledge support provided by DGAPA-UNAM) through Grant IN-115520 and CONACYT (Grant No. 284548). Technical assistance provided by Dr. Diego Delgado (UMAC-CICESE), Dr. Katrin Quester, E. Aparicio and F. Ruiz is gratefully acknowledged.

Conflicts of interest

There are no conflicts to declare

Keywords

Nanotechnology, biolabels, nanotoxicology, luminescent, nanoparticles.

Received: 10 June 2020

Revised: 21 June 2020

Accepted: 22 September 2020

References

- Bouzigues, C.; Gacoin, T.; Alexandrou, A.; *ACS Nano*, **2011**, *5*, 8488.
- Chatterjee, K.; Sarkar, S.; Jagajjani Rao, K.; Paria, S.; *Adv. Colloid Interface Sci.* **2014**, *209*, 8.
- Shan, J.; Chen, J.; Meng, J.; Collins, J.; Soboyejo, W.; Friedberg, J. S.; Ju, Y.; *J. Appl. Phys.* **2008**, *104*.
- MG, K.; V, K.; F, H.; *J. Nanomed. Nanotechnol.* **2015**, *06*.
- Tran, H. N.; Nghiem, T. H. L.; Vu, T. T. D.; Chu, V. H.; Le, Q. H.; Hoang, T. M. N.; Nguyen, L. T.; Pham, D. M.; Tong, K. T.; Do, Q. H.; Vu, D.; Nguyen, T. N.; Pham, M. T.; Duong, C. N.; Tran, T. T.; Vu, V. S.; Nguyen, T. T.; Nguyen, T. B. N.; Tran, A. D.; Trinh, T. T.; Nguyen, T. T. A.; *Adv. Nat. Sci. Nanosci. Nanotechnol.* **2015**, *6*.
- Kandarakis, I.; Cavouras, D.; Panayiotakis, G. S.; Koutsogiorgis, D.; Triantis, D.; Nomicos, C. D.; *HNPS Proc.* **2019**, *7*, 233.
- Padmanabhan, P.; Kumar, A.; Kumar, S.; Chaudhary, R. K.; Gulyás, B.; *Acta Biomater.* **2016**, *41*, 1.
- Chan, M.; Almutairi, A.; *Mater. Horizons* **2016**, *3*, 21.
- Kalaivani, S.; Guleria, A.; Kumar, D.; Kannan, S.; *ACS Appl. Bio Mater.* **2019**, *2*, 4634.
- Ansari, A. A.; Khan, A.; Labis, J. P.; Alam, M.; Aslam Manthrammel, M.; Ahamed, M.; Akhtar, M. J.; Aldabahi, A.; Ghaithan, H.; *Mater. Sci. Eng. C*, **2019**, *96*, 365.
- Isacfranklin, M.; Ameen, F.; Ravi, G.; Yuvakkumar, R.; Hong, S. I.; Velauthapillai, D.; AlKahtani, M. D. F.; Thambidurai, M.; Dang, C.; *Ceram. Int.* **2020**, *46*, 20553.
- Jain, K. K.; *The Handbook of Nanomedicine, Third Edition*, **2017**.
- Yang, Z.; Liu, Z. W.; Allaker, R. P.; Reip, P.; Oxford, J.; Ahmad, Z.; Reng, G.; *Nanotechnology, Brain, Futur.* **2013**, 313.
- Kang, H.; Mintri, S.; Menon, A. V.; Lee, H. Y.; Choi, H. S.; Kim, J.; *Nanoscale* **2015**, *7*, 18848.
- Alkilany, A. M.; Murphy, C. J.; *J. Nanoparticle Res.* **2010**, *12*, 2313.
- Park, S. Y.; Lee, C. Y.; An, H. R.; Kim, H.; Lee, Y. C.; Park, E. C.; Chun, H. S.; Yang, H. Y.; Choi, S. H.; Kim, H. S.; Kang, K. S.; Park, H. G.; Kim, J. P.; Choi, Y.; Lee, J.; Lee, H. U.; *Nanoscale* **2017**, *9*, 9210.
- Yu, Z.; Li, Q.; Wang, J.; Yu, Y.; Wang, Y.; Zhou, Q.; Li, P.; *Nanoscale Res. Lett.* **2020**, *15*.
- Goodman, C. M.; McCusker, C. D.; Yilmaz, T.; Rotello, V. M.; *Bioconjug. Chem.* **2004**, *15*, 897.
- Shukla, R.; Bansal, V.; Chaudhary, M.; Basu, A.; Bhonde, R. R.; Sastry, M.; *Langmuir* **2005**, *21*, 10644.
- Tsoli, M.; Kuhn, H.; Brandau, W.; Esche, H.; Schmid, G.; *Small*, **2005**, *1*, 841.
- Takahashi, H.; Niidome, Y.; Niidome, T.; Kaneko, K.; Kawasaki, H.; Yamada, S.; *Langmuir* **2006**, *22*, 2.
- Patra, H. K.; Banerjee, S.; Chaudhuri, U.; Lahiri, P.; Dasgupta, A. K.; *Nanomedicine Nanotechnology, Biol. Med.* **2007**, *3*, 111.
- Zhou, G.; Li, Y.; Ma, Y.; Liu, Z.; Cao, L.; Wang, D.; Liu, S.; Xu, W.; Wang, W.; *J. Nanoparticle Res.* **2016**, *18*, 1.
- Selvaraj, V.; Bodapati, S.; Murray, E.; Rice, K. M.; Winston, N.; Shokuhfar, T.; Zhao, Y.; Blough, E.; **2014**, *9*, 1379.
- Rajoria, S.; Rani, Chaudhari, D.; Jain, S.; Gupta, U.; *Pharm. Res.* **2019**, *36*.

26. Isakovic, A.; Markovic, Z.; Todorovic-Marcovic, B.; Nikolic, N.; Vranjes-Djuric, S.; Mirkovic, M.; Dramicanin, M.; Harhaji, L.; Raicevic, N.; Nikolic, Z.; Trajkovic, V.; *Toxicol. Sci.* **2006**, *91*, 173.
27. Sudimack, J.; Lee, R. J.; *Adv. Drug Deliv. Rev.* **2000**, *41*, 147.
28. Yee, K.; Seow, E.; Zhang, Y.; Chyn, Y.; *Biomaterials* **2013**, *34*, 4860.
29. Vu-Quang, H.; Vinding, M.S.; Nielsen, T.; Ullisch, M.G.; Nielsen, N.C.; Nguyen, D.T.; Kjems, J.; *Polymers (Basel)* **2019**, *11*.
30. Tahmasbi Rad, A.; Chen, C.-W.; Aresh, W.; Xia, Y.; Lai, P.-S.; Nieh, M.-P.; *ACS Appl. Mater. Interfaces* **2019**, *11*, 10505.
31. Cheung, A.; Bax, H. J.; Josephs, D. H.; Ilieva, K. M.; Pellizzari, G.; Opzoomer, J.; Bloomfield, J.; Fittall, M.; Grigoriadis, A.; Figini, M.; Canevari, S.; Spicer, J. F.; Tutt, A. N.; Karagiannis, S. N.; *Oncotarget* **2016**, *7*, 52553.
32. Costantino, L.; Tosi, G.; Ruozi, B.; Bondioli, L.; Vandelli, M. A.; Forni, F.; in *Nanoneuroscience and Nanoneuropharmacology* (Ed.: H.S.B.T.-P. in B.R. Sharma), Elsevier, **2009**, pp. 35-69.
33. Westin, S. N.; Sood, A. K.; Coleman, R. L.; in (Eds.: P.J. DiSaia, W.T. Creasman, R.S. Mannel, D.S. McMeekin, D.G.B.T.-C.G.O. (Ninth E. Mutch), Elsevier, **2018**, pp. 470-492.e10.
34. Chávez-García, D.; Juárez-Moreno, K.; Calderón-Osuna, I.; Navarro, P.; Hirata, G. A.; *J. Biomed. Mater. Res. - Part B Appl. Biomater.*, **2020**, *1*.
35. Taxak, V. B.; Khatkar, S. P.; Han, S.-D.; Kumar, R.; Kumar, M.; *J. Alloys Compd.* **2009**, *469*, 224.
36. Stöber, W.; Fink, A.; Bohn, E.; *J. Colloid Interface Sci.* **1968**, *26*, 62.
37. Chavez, D. H.; Juárez-Moreno, K.; Hirata, G. A.; *Nanobiomedicine* **2016**, *3*.
38. Chávez-García, D.; Juárez-Moreno, K.; Campos, C. H.; Alderete, J. B.; Hirata, G. A.; *J. Mater. Res.* **2018**, *33*.
39. Mosmann, T.; *J. Immunol. Methods* **1983**, *65*, 55.
40. Ivanov, V. M.; *J. Anal. Chem.* **2004**, *59*, 1002.
41. Chávez-García, D.; Juárez-Moreno, K.; Campos, C. H.; Tejada, E. M.; Alderete, J. B.; Hirata, G. A.; *J. Mater. Sci.* **2018**, *53*.
42. Malek Khachatourian, A.; Golestani-Fard, F.; Sarpoolaky, H.; Vogt, C.; Toprak, M. S.; *Ceram. Int.* **2015**, *41*, 2006.
43. Anh, T.; Benalloul, P.; Barthou, C.; Giang, L. T.; Vu, N.; Minh, L.; *J. Nanomater.* **2007**, *2007*, 26.
44. Gowd, G. S.; Patra, M. K.; Songara, S.; Shukla, A.; Mathew, M.; Vadera, S. R.; Kumar, N.; *J. Lumin.* **2012**, *132*, 2023.
45. Huang, X.; Guo, H.; *RSC Adv.* **2018**.
46. Hirata, D. D. G.A.; McKittrick, J.; Avalos-Borja, M.; Siqueiros, J.M.; *Appl. Surf. Sci.* **1997**, 509.
47. Xia, J.-M.; Wei, X.; Chen, X.-W.; Shu, Y.; Wang, J.-H.; *Microchim. Acta* **2018**, *185*, 205.
48. Blasse, B. C. G. G.; *Luminescent Materials*, **1994**.
49. Sonvico, F.; Dubernet, C.; Marsaud, V.; Appel, M.; Chacun, H.; Stella, B.; Renoir, M.; Colombo, P.; Couvreur, P.; *J. Drug Deliv. Sci. Technol.* **2005**, *15*, 407.
50. Stacey, G. N.; *Methods Mol Biol.*, **2011**, *731*, 79.
51. Weber, M.; Steinle, H.; Golombek, S.; Hann, L.; Schllensak, C.; Wendel, H. P.; Avci-Adali, M.; *Front. Bioeng. Biotechnol.* **2018**, *6*.
52. Wink, D. A.; Hines, H. B.; Cheng, R. Y. S.; Switzer, C. H.; Flores-Santana, W.; Vitek, M. P.; Ridnour, L. A.; Colton, C. A.; *J. Leukoc. Biol.* **2011**, *89*, 873.
53. Liang, H.; Nacharaju, P.; Friedman, A.; Friedman, J. M.; *Futur. Sci. OA* **2015**, *1*, FSO54.
54. Hsiao, I.-L.; Hsieh, Y.-K.; Wang, C.-F.; Chen, I.-C.; Huang, Y.-J. *Environ. Sci. Technol.* **2015**, *49*, 3813.
55. Silver, J. H.; *J. Neurol. Neurophysiol.* **2011**, *01*, 1.
56. Manke, A.; Wang, L.; Rojanasakul, Y.; *Biomed Res. Int.* **2013**, *2013*.
57. Oesch, F.; Landsiedel, R.; *Arch. Toxicol.* **2012**, *86*, 985.
58. Suzuki, H.; Toyooka, T.; Ibuki, Y.; *Environ. Sci. Technol.* **2007**, *41*, 3018.
59. Kumar, A.; Pandey, A. K.; Singh, S. S.; Shanker, R.; Dhawan, A.; *Cytometry. A* **2011**, *79*, 707.
60. Subik, K.; Lee, J.-F.; Baxter, L.; Strzepak, T.; Costello, D.; Crowley, P.; Xing, L.; Hung, M.-C.; Bonfiglio, T.; Hicks, D. G.; Tang, P.; *Breast Cancer (Auckl)*. **2010**, *4*, 35.

Authors biography



Dr. Dalia Chávez holds Ph.D in Physics of Materials from CICESE-UNAM in Ensenada, Mexico; M.Sc in Engineering from CETYS University and a B.S. in mechanical engineering from ITESM in Moterrey, Mexico. She is actually the dean of engineering at CETYS University. Her work experience is in the areas of professor of engineering programs, scientific research in nano-biotechnology and materials science and arranging/organized research conferences, seminars, workshops and events. Also she had several research publications in well-known international journals and conferences related to nanotechnology, materials science and engineering.



Dr. Karla Juárez-Moreno holds a Ph.D. in Biotechnology from CICESE-UNAM in Ensenada, Mexico. She is an Associate Researcher from Catedras CONACYT and part of the Bionanotechnology Department of the Center of Nanoscience and Nanotechnology from the National Autonomous University of Mexico. Her work is related to Nanotoxicology and Bionanotechnology, focusing on the study of cellular responses to nanomaterials. She is part of the National System for the Toxicological Evaluation of Nanomaterials (SINANOTOX, Mexico) and member of the CaliBaja Center for Resilient Materials (UCSD, USA).



Dr. Gustavo A. Hirata is a Mexican physicist who has made many contributions to the field of nanotechnology, physics and materials science. His research has focused on the correlation of structure and properties of luminescent materials and nanophosphors with applications in solid state white-emitting lamps and nanomedicine. The present focus of his research work is to develop novel nanophosphors to increase the efficiency in solar cells.



Rosella Reyes is currently studying a bachelor's degree in Mechatronics Engineering at CETYS University. She is actually working as assistant of synthesis of nanoparticles for detection of cancer cells, she is also a member of the Engineering Student Council and the finance coordinator in FORTES, a leadership program that is part of the United Nations Academic Impact. She took an Intercultural Leadership Seminar at Fairleigh Dickinson University and a course in Engineering Economics and Professionalism in CSUF.



Juan Barrera has a bachelor degree in mechatronics engineering for, CETYS university, he worked in the synthesis of down and upconversion nanoparticles for detection of cancer cells, he participated in Engineering Together Sustainable Communities 2017 in collaboration with the University of UTEP, improving the applied methods to obtain natural resources used in the vineyard.

Graphical abstract

DCNPs-FA

